LA-UR- 99-869

*Approved for public release; distribution is unlimited.*

*Title:* THUNDERSTORM AND LIGHTNING STUDIES USING THE FORTE OPTICAL LIGHTNING SYSTEM (FORTE/OLS)



*Author(s):* D.M. Suszcynsky, NIS-1
M. Kirkland, NIS-1
P. Argo, NIS-1
R. Franz, NIS-4
A.R. Jacobson, NIS-1
S. Knox, NIS-1
J.L. Guillen, Sandia Natioanl Laboratories
J. Green, Sandia National Laboratories

*Submitted to:* 11th International Conference on Atmospheric Electricity, June 7-11 1999, Guntersville, AL

**Los Alamos**
NATIONAL LABORATORY

# Thunderstorm and Lightning Studies Using the FORTE Optical Lightning System (FORTE/OLS)

D. M. Suszcynsky, M. Kirkland, P. Argo, R. Franz, A. R. Jacobson, S. Knox
*Los Alamos National Laboratory, Space & Atmospheric Sciences Group, MS D466, Los Alamos, NM 87545*

J. L. Guillen, J. Green, R. Spalding
*Sandia National Laboratories, Sensors and Electronics Dept., MS 0972, Albuquerque, NM 87185*

## ABSTRACT

Preliminary observations of simultaneous RF and optical emissions from lightning as seen by the FORTE spacecraft are presented. RF/optical pairs of waveforms are routinely collected both as individual lightning events and as sequences of events associated with cloud-to-ground (CG) and intra-cloud (IC) flashes. CG pulses can be distinguished from IC pulses based on the properties of the RF and optical waveforms, but mostly based on the associated RF spectrograms. The RF spectrograms are very similar to previous ground-based VHF observations of lightning and show signatures associated with return strokes, stepped and dart leaders, and attachment processes,. RF emissions are observed to precede the arrival of optical emissions at the satellite by a mean value of 280 microseconds. The dual phenomenology nature of these observations are discussed in terms of their ability to contribute to a satellite-based lightning monitoring mission.

## INTRODUCTION

Space-based observations of lightning and thunderstorms in both the radio frequency (e.g. *Herman et al.*, [1965]; *Holden et al.*, [1995]; *Horner and Bent*, [1969]; *Kotaki and Katoh*, [1983]; *Leiphart et al.*, [1962]; *Massey and Holden*, [1995]) and optical (e.g. *Sparrow and Ney*, [1971]; *Turman*, [1978]; *Vonnegut et al.*, [1983]; *Vorpahl et al.*, [1970]) parts of the electromagnetic spectrum have been made since the 1960s (see also the review by *Goodman and Christian* [1993]). However, apart from a few brief experiments using the Global Positioning System's Nuclear Detonation System (GPS/NDS) in the 1990s, and limited use of a fast photodiode in conjunction with the BLACKBEARD RF experiment aboard the ALEXIS satellite (e.g. *Holden et al.*, [1995]), no specifically designed space-based efforts have been mounted to simultaneously observe optical and radio frequency (RF) emissions from lightning on a routine, automated basis. The importance of performing such a study is clear. A dual phenomenology approach to lightning observations from space might significantly contribute to our eventual ability to monitor and remotely identify lightning types (cloud-to-ground, intra-cloud, etc.) from satellites. This has significant implications for planned NASA missions to eventually monitor lightning activity from geosynchronous orbit (*Goodman et al.*, [1988]; *Christian et al.*, [1989]). In addition, dual rf/optical observations of lightning from satellites can also provide unique data sets from which to study the basic physics of lightning on a global scale.

In remedy of this situation, the Fast On-Orbit Recording of Transient Events (FORTE) satellite was launched on Aug. 29, 1997. FORTE is a joint Los Alamos National Laboratory and Sandia National Laboratories satellite experiment that was primarily designed to address technology issues associated with treaty verification and the monitoring of nuclear tests from space. The satellite carries VHF broadband radio receivers and an Optical Lightning System (OLS) that are optimally designed for the detection of lightning transients. The design of this instrumentation and its availability for continuous scientific use make FORTE an ideal space platform from which to monitor and study the simultaneous emission of RF and optical radiation from lightning.

## INSTRUMENTATION

FORTE is situated in a nearly circular, 70°-inclination orbit of approximately 825-km altitude with an orbital period of about 100 minutes. The instrumentation used for this study includes the two narrower-band FORTE VHF receivers as described in *Jacobson et al.*, [1998], and the Photodiode Detector (PDD) of the FORTE OLS which is described in *Kirkland et al.*, [1998].

The RF instrumentation consists of two VHF broadband receivers that can each be independently configured to cover a 22-MHz sub-band in the 30 - 300 MHz frequency range. For this study, one receiver was chosen to span the 26 - 48 MHz range and the other spanned the 118 - 140 MHz range. The instruments were configured to collect 40960 samples in a 800 microsecond record length resulting in a time resolution of 20 nano-seconds (sample rate of 50 Msa/sec). The trigger point in each record allowed for 500 microseconds of pre-trigger information and 300 microseconds of post-trigger information. The record length and pre/post trigger intervals were chosen to optimize the detection and identification of the rf lightning emissions. Data collection was triggered off the lower (26 - 48 MHz) band receiver when the amplitude of its detected signal exceeded a preset noise-riding amplitude threshold in at least five of eight 1-MHz wide sub-bands distributed throughout the 22-MHz bandwidth (*Jacobson et al.*, [1998]). This triggering technique allows the instrument to trigger on and detect weak lightning signatures in the presence of strong interfering manmade carriers. Retriggering can occur after only a few microsecond delay allowing the instrument to record extended multi-record signals with essentially zero dead-time. The "field-of-view" of the VHF receivers is determined by the antenna pattern, the 3-dB attenuation boundary being an approximate circle of about 1200 km diameter and chosen to approximately correspond to the field-of-view of the PDD.

The PDD is a broadband (0.4 - 1.1 micron) silicon photodiode detector that collects amplitude versus time waveforms of lightning transients. The instrument has an 80-degree field-of-view which translates into a footprint of about 1200-km diameter for an 825-km altitude orbit. The instrument is typically configured to produce 1.92 millisecond records with 15 microsecond time resolution. The PDD is typically amplitude-threshold triggered, with a noise-riding threshold, and with a requirement that the signal exceed the amplitude threshold for 5 consecutive samples before triggering occurs. This protocol eliminates false triggers due to energetic particles and noise. However, the instrument can also be slaved to the VHF receivers whereby a trigger is forced whenever a VHF signal is received. The PDD provides 12-bit sampling with a piece-wise linear dynamic range covering 4 orders of magnitude and a sensitivity of better than $10^{-5}$ watts/$m^2$. Several background compensation modes allow the instrument to be operated both at night and at a reduced sensitivity in the day. Because of a circular buffer scheme, the PDD has a

dead-time of about 3 to 4 milliseconds after the collection of a trigger. The start of both the VHF and PDD records are GPS-time-stamped to a 1 micro-second accuracy.

## OBSERVATIONS AND ANALYSIS TECHNIQUES

The inspection of a typical correlation case for a CG flash ( figure 1) demonstrates the basic phenomenology of the rf/optical correlations. Figure 1a shows a sequence of 4 consecutive PDD triggers that occur over a 0.25 second time interval. The vertical spikes are actual PDD waveforms that appear compressed because of the large time scale displayed. The red triangles mark the reported times of three strokes of a three-stroke -CG flash as identified by National Lightning Detection Network data. Figure 1b shows a corresponding sequence of three consecutive RF waveforms that were collected over the same time interval. As can be seen, the FORTE data set captures the majority of the rf and optical pulses emitted from the CG flash as identified by the NLDN data. Figure 1cde present the detailed comparison of the three rf/optical pairs in the flash. The rf waveforms are displayed on an arbitrary amplitude scale to facilitate time comparisons with the optical waveforms. In each case the rf trigger is seen to precede the optical trigger by tens to a few hundreds of microseconds, depending on how the time delay is measured. Figure 1fgh show the rf spectrograms for the three rf records displayed in figure 1cde. The spectrograms were generated by taking 256-sample Blackman-windowed fast fourier transforms of the waveform as the window was moved in 16- sample increments through the record. The spectrograms plot the signal power expressed in dBm (color bar) as a function of frequency and time and show features that are uniquely characteristic of CGs (see discussion section). The arrows in figure 1fgh indicate the NLDN-reported stroke times which are corrected for propagation delays to the satellite by using the NLDN source locations, the satellite location, and an ellipsoid model of the earth.

The degree to which the rf signal precedes the optical signal is an important parameter to measure since the delay in the arrival of the optical signal at the satellite can be related to the mean scattering delay of light propagating through clouds (e.g. *Thomason and Krider*, [1982]). An experimental determination of this number can be used to "truth" existing light propagation models but is complicated by the fact that the delays may also be influenced, in part, by any natural delay between the rf and optical emissions from the source. Unless ground truth is available, it can be difficult to assess this contribution to the total delay. As a first step in deducing the mean scattering delay due to clouds, a subset of rf/optical correlation data was analyzed to remove the biases (i.e. triggering and thresholding biases) that are introduced by considering trigger time differences rather than true signal arrival time differences (i.e. correlation times). Because of the complex and variable nature of both the rf and optical waveforms, the true correlation times, $\Delta t_{corr}$, were analyzed and measured by hand, a laborious process that resulted in a much more limited, but more physically meaningful, data set.

The analysis procedure is to determine $\Delta t_{scatt}$ by measuring the amount of pulse broadening. This value is then subtracted from the $\Delta t_{corr}$ measurement to also arrive at an estimate for $\Delta t_{phys}$. For this study, $\Delta t_{corr}$ was determined by measuring the interval between the start time of the RF pulse and the peak time of the associated optical pulse. This method introduces an inherent uncertainty in the measured delay on the order of the risetime of the current pulse (1 -10 microseconds), but this is small compared to the measured $\Delta t_{corr}$ values. These measurement points were chosen because they correspond to features in both the rf and optical records that are unambiguously identifiable, and at the same time, physically meaningful.

Figure 2 shows a histogram of $\Delta t_{corr}$ as measured with the above technique for a subset of 237 rf/optical pairs of triggers. The pairs were randomly selected during a three week period of data collecting over the continental United States and bordering regions and includes the observation of well over 40 storms. RF record lengths of 800 microseconds with 500 microseconds of pre-trigger time were used to assure that the rf triggers were of isolated events and not just one small interval of a more extensive emission. The uncertainty in each measurement of $\Delta t_{corr}$ is estimated to be about +/- 25 microseconds and reflects uncertainties in properly identifying the rf start time and the PDD peak time. The mean value of the measured $\Delta t_{corr}$ is -282 microseconds where the minus sign indicates that the rf signal precedes the optical signal. The measured $\Delta t_{corr}$ for the three rf/optical pairs are indicated on the tops of figures 1cde. In keeping with measurement convention, a $\Delta t_{corr}$ for the rf/optical pair shown in figure 1d was not measured since the optical signal is highly structured. The chosen rf start times and optical peak times are indicated by red arrows in figure 1cdefh. As can be seen, there is some choice in where to mark the rf start time. The strategy is to choose the rf start time of that part of the rf signal which corresponds to the same phenomena that produces the optical emission. For both initial and subsequent return strokes, the rf start time is chosen to correspond to the start of the actual return stroke. The rationale and vindication for this choice is described in the discussion section. An important observation concerning the 237 measured cases is that 228 of them ( 131 confirmed by NLDN and 97 inferred from the spectrogram patterns) were associated with CGs. For the 13nn cases that were associated with IC's (identified by the impulsive signatures in the RF spectrograms), accurate $\Delta t_{corr}$ 's were not measured because a unique RF start point and/or optical peak could not be identified.

Figure 2 also contains a second histogram in red that shows the results of the broadening measurement. In order to compare this result with the $\Delta t_{corr}$ measurements, we calculated the effective pulse width for the 237 cases as described above, subtracted 200 microseconds which represents the source *mean* effective pulse width for CGs as measured from the ground by *Mackerras et al.*, [1965] *and Guo and Krider*, [1982], and then took the negative of the result to facilitate comparison with the $\Delta t_{corr}$ measurements. As is shown in figure 2, the mean broadening (i.e. $\Delta t_{scatt}$) is about 143 microseconds, which equates to a 33 kilometer additional photon path length. The mean value for $\Delta t_{phys}$ is then calculated as $\Delta t_{corr} - \Delta t_{scatt} = 282$ microseconds - 143 microseconds $\cong$ 139 microseconds.

## DISCUSSION

The identification of the various lightning features in figures 1 is somewhat speculative since adequate ground truth, specifically radiation waveforms with the proper time resolution, is lacking. The NLDN data offers some ground truth on return strokes although it must be kept in mind that NLDN does not provide waveforms and employs an LF/VLF magnetic field direction-finding system as opposed to the FORTE receivers which measure broadband VHF radiation. No optical ground truth was available for the study. An additional consideration for the detection of the VHF is that the look direction for the FORTE sensors is generally parallel to the channel current flow while that of ground-based measurements is generally perpendicular. Consequently, any directionality in lightning VHF emissions might result in significantly different signatures observed by FORTE as opposed to ground measurements. Despite these limitations, the routine association of certain FORTE/rf signatures with certain types of NLDN-verified activity, as is shown in figure 1, provides us with some degree of confidence in tentatively assigning interpretations to the features in the spectrograms. This confidence is

further supported by striking similarities between the FORTE VHF data and previous ground-based measurements and identifications of HF and VHF emissions from various phases of CG activity (e.g. *Brook and Kitagawa*, [19xx]; *Levine and Krider*, [1977]; *Hayenga*, [1984]; *Rhodes et al.*, [19xx]; *Shao et al.*, [1995], *Mazur et al.*, [1995]).

Figure 1fgh contains spectrogram patterns that are typical for those associated with CG flashes. The choices for the rf start times in figure 1fgh are highly dependent upon the physical interpretations of the spectrograms and vice versa. Consequently, the analysis approach was one of iteration, culminating when a self-consistent interpretation was attained between the FORTE rf and optical observations, the corresponding NLDN data, and the bibliography of previous ground-based interferometer measurements. The broadband signal in the first 500 microseconds of the spectrogram in figure 1f (initial return stroke) is tentatively identified as stepped leader emission and is immediately followed by an additional 100 microsecond burst of radiation that is most likely associated with the subsequent propagation of the return stroke current. The attachment process then, presumably occurs at the boundary between these two regions. This identification of first return stroke features is supported by several observations: (1) the NLDN detection of the onset of the return stroke occurs at the end of the purported leader emission and at the beginning of the burst associated with the return stroke as expected, (2) ground-based interferometer measurements of first return strokes show similar features that agree with those in figure 1f in terms of relative intensity and timing, (3) the time durations of the purported leader (always greater than 500 microseconds) and return stroke emissions ( ~ 100 microseconds) are consistent with those measured on the ground, (4) unlike subsequent return strokes, first strokes typically display significant branching which is believed to result in VHF emissions [ref] during the actual return stroke as is observed, and (5) as will be seen below, the measured $\Delta t_{corr}$ is consistent with the feature identification.

In order to choose the right rf start time to associate with the corresponding optical signature, we make the assumption that the detected optical signal for first strokes is associated with the actual return stroke process and that any optical emissions related to the stepped leader are too weak to be detected. This assumption is vindicated, for example, by the measurements of *Goodman and Christian*, [1988] in which optical emissions from stepped leaders were not detectable by photodiodes mounted in an aircraft above thunderstorm clouds. We therefore choose the rf start time at the attachment point.

The two spectrograms shown in figure 1gh are typical of subsequent strokes and display an initial interval where the VHF increases in intensity followed by either a steady decrease in intensity (figure 1dg) or a more common sudden turn-off of emission (figure 1eh). The time duration of the entire RF emission associated with subsequent strokes is typically 100 - 400 microseconds. In both spectrograms, we identify the entire signal as due to dart leader emission. The sudden turn-off of VHF in figure 1eh corresponds to the start of the return stroke and the gradual turn-off of radiation in figure 1dg is currently unexplained. This identification of subsequent return stroke features is supported by the following observations: (1) the NLDN detection of the onset of the subsequent return stroke occurs at the end of the purported dart leader emission as expected, (2) ground-based interferometer measurements of subsequent return strokes show similar features that agree with those in figure 1gh in terms of relative intensity and timing, (3) the time durations of the purported dart leader (typically 100 - 400 microseconds) is consistent with those measured on the ground, (4) the cessation of radiation at the onset of the subsequent stroke is in agreement with ground measurements, and (5) as will be seen below, the measured $\Delta t_{corr}$ is consistent with the feature identification.

For subsequent return strokes, as in figure 1gh, the choice of where to place the rf start time is somewhat more difficult since the spectrogram signatures are slightly more variable than those for initial strokes. Dart leaders are strong VHF emitters (e.g. *Hayenga,* [1979]*; Levine and Krider*, [1977]) and are known to have a significant optical output that is typically on the order of 10 % of that associated with the actual return stroke (*Idone and Orville*, [1985]). Such a signal may be detectable by the PDD but at a much reduced amplitude as compared to the emission associated with the actual return stroke current. Consequently, we assume that the dart optical emission will contribute little to the overall signal detected by the PDD and therefore measure the rf start time for a subsequent stroke at the beginning of the return stroke (ie the end of the dart leader emission). A measurement of the ratio of the rise time to the fall time of the optical signature for subsequent strokes versus initial strokes does indicate that subsequent stroke optical waveforms are slightly more symmetic than those for initial return strokes. This may be an indicator of a weak optical contribution by the dart leader to the overall waveform; however such a contribution would not significantly affect the $\Delta t_{corr}$ measurement as defined. Finally, ground-based measurements also often report a gap on the order of ~100 microseconds between the VHF emisssions associated with the dart leader and those associated with the in-cloud activity that usually follows the propagation of the return stroke [ref]. We sometimes see an enhancement of VHF emission 100 - 200 microseconds after the return stroke, although this is typically not the case.

A more detailed analysis that quantifies the rf spectrogram and optical characteristics for different types of lightning is ongoing and will be reported on in a subsequent paper. However, it is already clear from this initial analysis that an analysis of rf signatures of lightning in tandem with optical data can greatly enhance a satellite's ability to discriminate lightning types from space. Some discrimination information can be found in the optical waveforms, namely the slight asymmetry in first stroke waveforms as compared to subsequent strokes and the weaker amplitude, broader, and more highly structured nature of IC waveforms as compared to CG waveforms. However, the bulk of the discrimination capability in the FORTE instruments seems to lie in the interpretation of the RF spectrograms. Based on the 143 NLDN-corroborated cases from the data shown in figure 2, we find that we can distinguish between initial return strokes, subsequent return strokes and intra-cloud discharges at a better than 90% confidence level.

The values for $\Delta t_{phys}$ and $\Delta t_{scatt}$ that were deduced from the measurements in figure 2 can be compared to various models and experimental data. Ground-based interferometer measurements in tandem with optical observations indicate that the strongest RF near the time of initial return strokes occurs during the attachment process and that this emission typically precedes the peak of the subsequent optical emission by 50 - 100 microseconds. Since the light output of a return stroke is proportional to the total channel length (REF), the peak optical emission should when the length of the return stoke is at a maximum, i.e. when the stroke reaches the cloud. The $\Delta t_{phys}$ = 140 microsecond measurement actually suggests a source that emits just after this point, probably the in-cloud phase of optical activity that follows the return stroke. Likewise, for subsequent strokes, $\Delta t_{phys}$ is comparable in value to the time delay seen between the initiation of the subsequent return stroke and the in-cloud activity that follows. These comparisons imply that the FORTE-detected VHF from CGs is sourced to the attachment process or beginning of the return stroke, while the FORTE-detected light from CGs is primarily sourced to the in-cloud portion of the return stroke.

A comparison between the measured mean of $\Delta t_{scatt}$ and predictions from various cloud scattering models is generally difficult since the initial conditions of the models do not always match up to the existing conditions during the FORTE measurements. And likewise, the existing cloud and source conditions during the FORTE measurements are not well understood particularly in the absence of ground truth. However, the measured mean $\Delta t_{scatt}$ of 138 microseconds compares favorably to the results of *Thomason and Krider*, [1982]. The *Thomason and Krider*, [1982] model for light propagation through clouds is a Monte Carlo method that simulates Mie scattering processes driven by homogenous clouds of various dimensions and particle-size compositions. The model is particularly applicable to the FORTE data set since it considers light scattering and absorption of impulsive point source emissions placed at various locations within finite geometric clouds. For a light transient sourced at the center of a cloud of optical depth 200 and water drop diameter of 10 microns (moderate maritime cumulonimbus), the model predicts a mean scattering delay of about 51 microseconds (xx km increased path length) while the predicted value for an optical depth of 400 (strong maritime cloud) is 130 microseconds (yy km increased path length). The $\Delta t_{scatt}$ result of figure 2 compares less favorably to the recent xte measurements of Philsticker et al (1998) that show a scattering delay on the order of 350 microseconds for two observed cumulonimbus thunderstorm clouds of 5 km vertical extent. However, these values were for transmission of light from a source above the clouds (the sun) to the detector below the clouds and tend to significantly overestimate the additonal path length that one would expect for a source near the center of the cloud, as would be the case for IC lightning or the in-cloud components of return strokes.

$\langle \Delta t_{scatt} \rangle$ was estimated to be greater than 447 microseconds (114 kms) by *Kirkland et al.*, [1998] using the full FORTE/PDD data set. This value is marked as a vertical dashed line in figure 2 and is significantly greater than the mean of the $\Delta t_{scatt}$ histogram in figure 2. The discrepency between the 447 microsecond *Kirkland et al.*, [1998] result and the 143 microsecond result of this study is apparently a function of lightning type. *Kirkland et al.* [1998] did not distinguish between CG and IC-sourced light. Since IC pulses are the predominant type of lightning and since the IC light signals detected by FORTE are generally broader and more structured than those associated with CGs, the inclusion of IC light in the *Kirkland et al*, [1998] statistics tends to bias the estimate for the mean scattering delay to larger values than those associated with just CGs. In fact, when the Kirkland et al. [1998] analysis is redone to include only those PDD triggers for which there was a NLDN CG report, we find a mean effective pulse width of approximately ddd microseconds, much closer to the 143 microsecond value measured for this study (*Kirkland et al.*, [1999]).

## ACKNOWLEDGEMENTS

The authors would like to thank Paul Kreihbel of The New Mexico Institute of Mining and Technology, and Anthony Davis, Dott Delapp, Bob Roussel-Dupre, Diane Roussel-Dupre, Ken Eack, Dan Holden, Phil Klingner, Charley Rhodes, Xiaun-Min Shao, and Dave Smith of Los Alamos National Laboratory for useful discussions, comments, and support during this study. This work was supported by the United States Department of Energy.

## REFERENCES

Beasley, W. H., M. A. Uman, D. M. Jordan, and C. Ganesh, Simultaneous pulses in light and electric field from stepped leaders near ground level, *J. Geophys. Res., 88*, 8617-8619, 1983.

Christian, H. J., R. J. Blakeslee, and S. J. Goodman, The detection of lightning from geostationary orbit, *J. Geophys. Res., 91*, 13329-13337, 1989.

Ganesh, C., M. A. Uman, W. H. Beasley, and D. M. Jordan, Correlated optical and electric field signals produced by lightning return strokes, *J. Geophys. Res., 89*, 4905-4909, 1984.

Gomes, C., and V. Cooray, Correlation between the optical signatures and current waveforms of long sparks: applications in lightning research, *J. Electrost., 43*, 267-274, 1998.

Goodman, S. J., H. J. Christian, and W. D. Rust, A comparison of the optical pulse characteristics of intracloud and cloud-to-ground lightning as observed above clouds, *J. Applied Meteor., 27*, 1369-1381, 1988.

Goodman, S. J. and H. J. Christian, Global Observations of Lightning, in Atlas of Satellite Observations Related to Global Change, 1993.

Guo, C. and E. P. Krider, The optical and radiation field signatures produced by lightning return strokes, *J. Geophys. Res., 87*, 8913-8922, 1982.

Hayenga, C. O., Characteristics of lightning VHF radiation near the time of the return stroke, *J. Geophys. Res., 89*, 1403-1410, 1984.

Herman, J. R., J. A. Caruso, and R. G. Stone, Radio astronomy explorer (RAE-1), observation of terrestrial radio noise, *Planet. Space Sci., 21*, 443-461, 1965.

Holden, D. N., C. P. Munson, and J. C. Devenport, Satellite observations of transionospheric pulse pairs, *Geophys. Res. Lett., 22(8)*, 889-892, 1995.

Horner, F. and R. B. Bent, Measurement of terrestrial radio noise, *Proc. Roy. Soc. A, 311*, 527-542, 1969.

Idone, V. P. and R. E. Orville, Correlated peak relative light intensity and peak current in triggered lightning subsequent return strokes, *J. Geophys. Res., 90*, 6159-6164, 1985.

Jacobson, A. R., S. O. Knox, R. Franz, D. C. Enemark, FORTE observations of lightning radio-frequency signatures: capabilities and basic results, submitted to *Radio Sci.*, 1998.

Kirkland, M. W., D. M. Suszcynsky, R. Franz, J. L. L. Guillen, J. L. Green, Observations of terrestrial lightning at optical wavelengths by the photodiode detector on the FORTE satellite, submitted to *J. Geophys. Res.*, 1998.

Kirkland et al., PDD/NLDN Comparisons, 1999.

Kotaki, M. and C. Katoh, The global distribution of thunderstorm activity observed by the ionosphere sounding satellite (ISS-b), *J. Atmos. And Terr. Physics, 45*, 833-847, 1983.

## FIGURE CAPTIONS

Figure 1. Example of an NLDN-confirmed -CG flash. (a) consecutive PDD waveforms collected over a 0.25 second time interval with NLDN-detected strokes identified by red triangles, (b) consecutive VHF waveforms collected over the same time interval as in (a), (cde) expanded plots of the three rf/optical waveform pairs shown in (a) and (b), (fgh) frequency-time spectrograms of the three VHF waveforms shown in (cde).

Figure 2. $\Delta t_{corr}$ and $\Delta t_{scatt}$ measurement histogram.

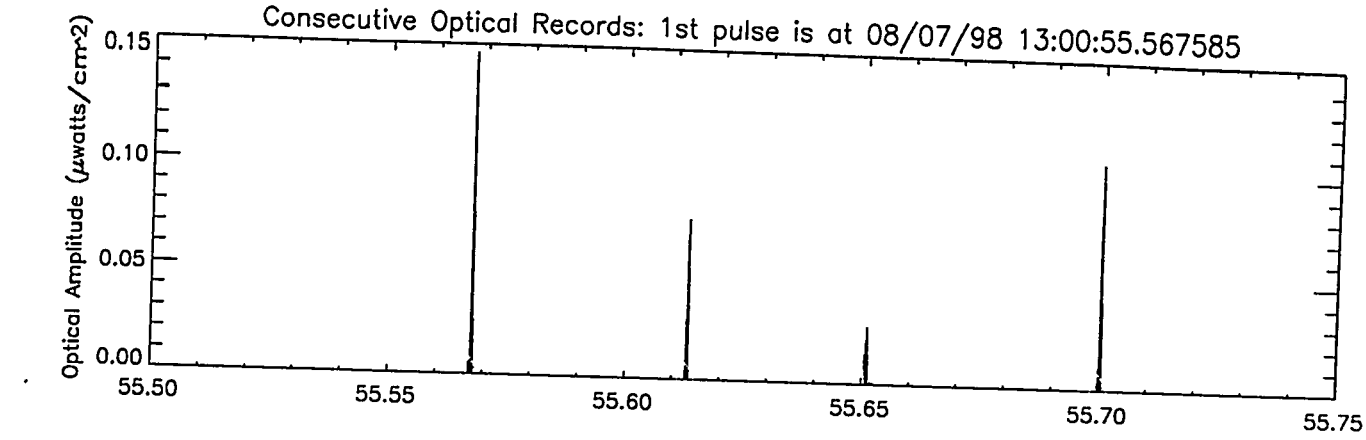
Consecutive Optical Records: 1st pulse is at 08/07/98 13:00:55.567585
Optical Amplitude (μwatts/cm^2)
0.15
0.10
0.05
0.00
55.50
55.55
55.60
55.65
55.70
55.75

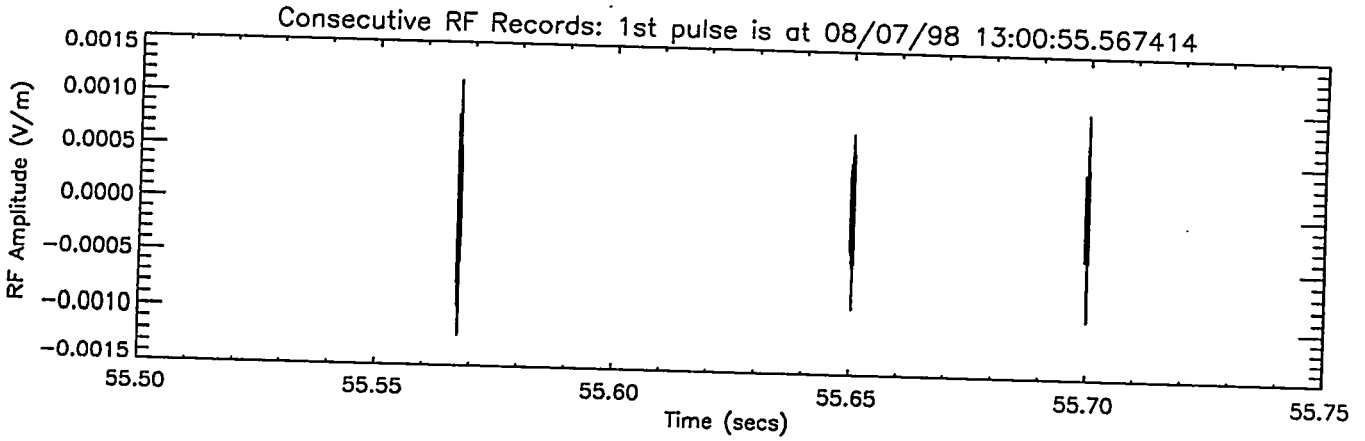
Consecutive RF Records: 1st pulse is at 08/07/98 13:00:55.567414
RF Amplitude (V/m)
0.0015
0.0010
0.0005
0.0000
−0.0005
−0.0010
−0.0015
55.50
55.55
55.60
55.65
55.70
55.75
Time (secs)

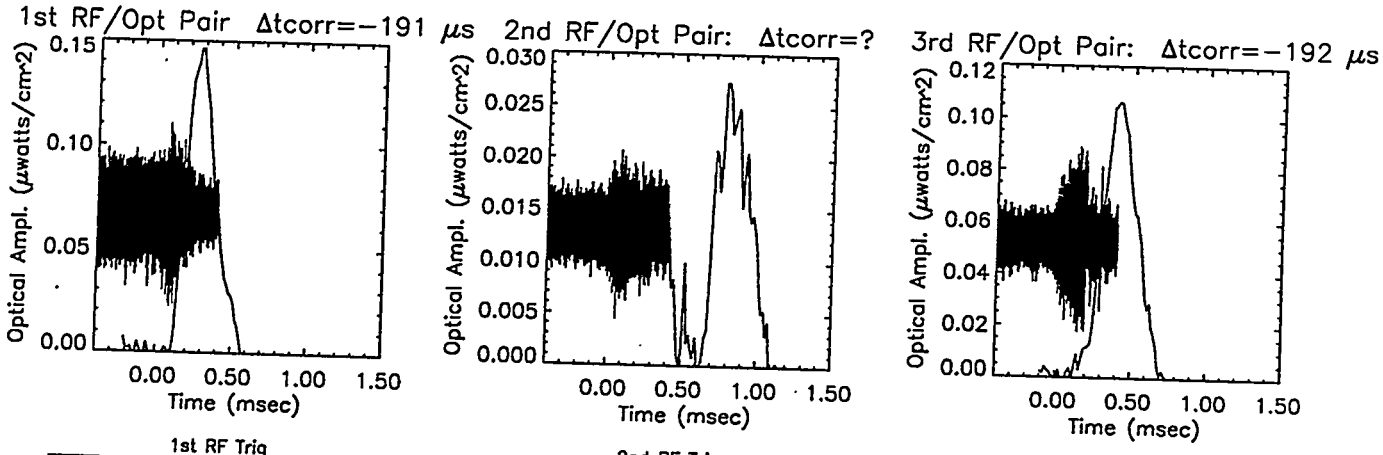
1st RF/Opt Pair Δtcorr=−191 μs
2nd RF/Opt Pair: Δtcorr=?
3rd RF/Opt Pair: Δtcorr=−192 μs
Optical Ampl. (μwatts/cm^2)
Time (msec)
0.00
0.50
1.00
1.50

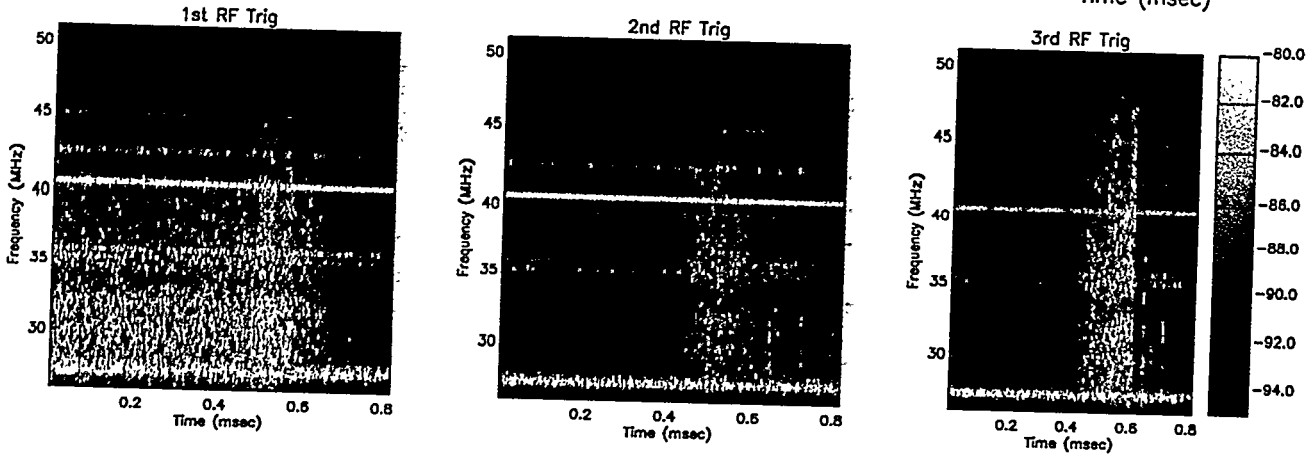
1st RF Trig
2nd RF Trig
3rd RF Trig
Frequency (MHz)
Time (msec)
50
45
40
35
30
0.2
0.4
0.6
0.8
−80.0
−82.0
−84.0
−86.0
−88.0
−90.0
−92.0
−94.0

Figure 1

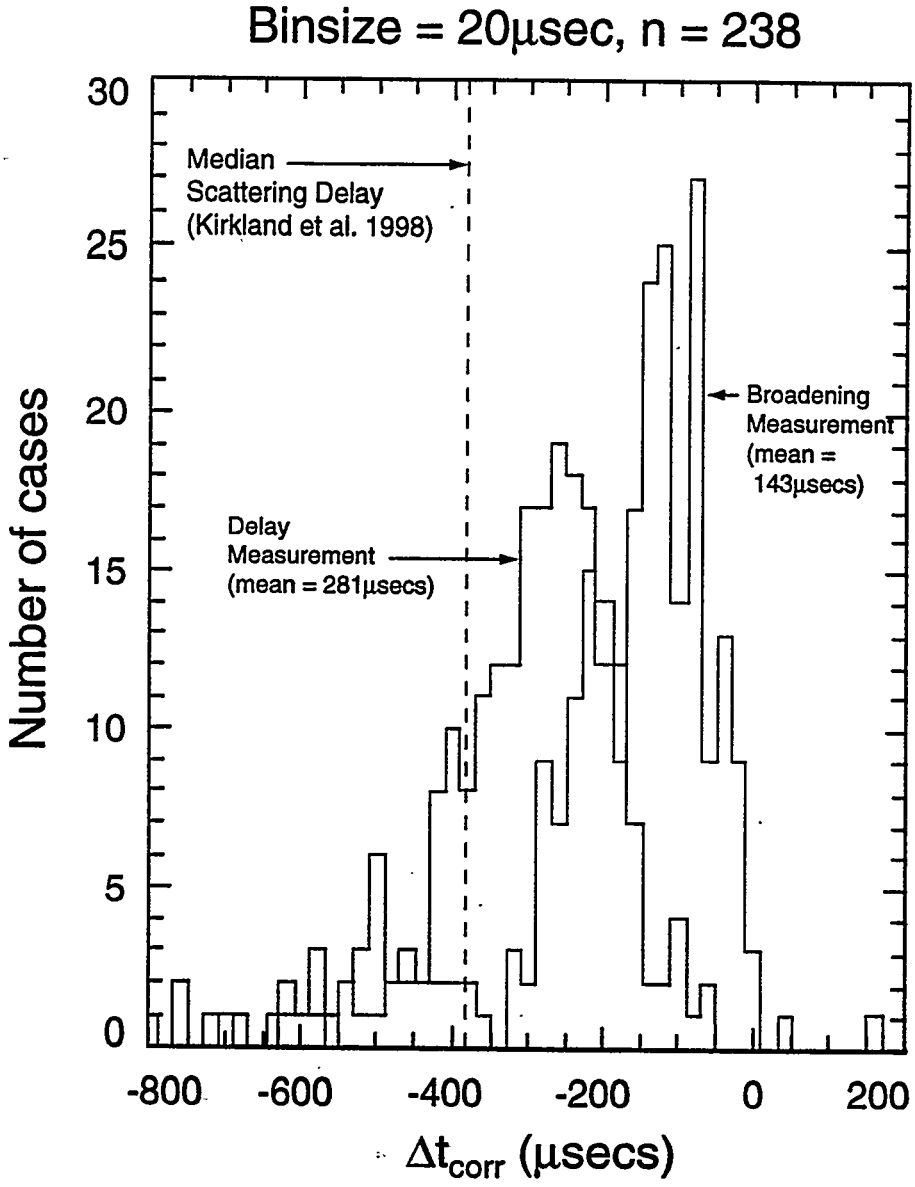
Binsize = 20μsec, n = 238
Number of cases
30
25
20
15
10
5
0
-800
-600
-400
-200
0
200
Δt_corr (μsecs)
Median
Scattering Delay
(Kirkland et al. 1998)
Delay
Measurement
(mean = 281μsecs)
Broadening
Measurement
(mean =
143μsecs)